THE JOURNAL OF PHYSICAL CHEMISTRY B

Article

pubs.acs.org/JPCB

Preparational Effects on the Excitation Energy Transfer in the FMO Complex

Lothar Mühlbacher*,† and Ulrich Kleinekathöfer*,‡

†Physikalisches Institut, Albert−Ludwigs−Universität Freiburg, Hermann-Herder-Str. 3, 79104 Freiburg, Germany

‡School of Engineering and Science, Jacobs University Bremen, Campus Ring 1, 28759 Bremen, Germany

ABSTRACT: Using numerically exact path integral Monte Carlo simulations, the excitation energy transfer in the Fenna−Matthews−Olson (FMO) complex is determined at room temperature. The employed system and environment parameters are based on previously reported atomistic simulations. When starting with excitations localized at specific chromophores, no coherence features can be observed. In contrast, when starting with delocalized excitations, traces of coherent motion become apparent. On the one hand, as experimental findings account for much stronger quantum coherent motion, these results suggest a reevaluation of the underlying spectral densities. On the other hand, the results emphasize that the initial preparation of the excitonic system needs to be taken into account carefully when attempting to reproduce the respective experiments.

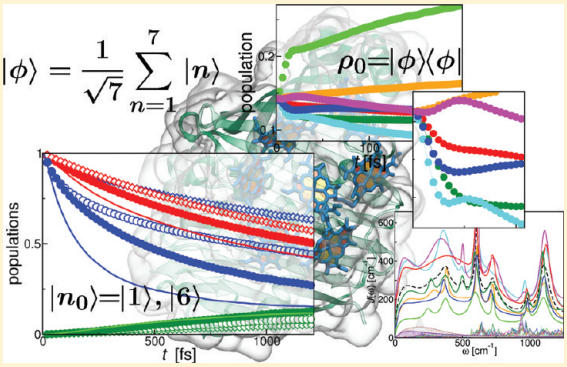

INTRODUCTION

Since the seminal experiments on the Fenna−Matthews−Olson (FMO) complex in which long-lived quantum coherences were observed,[1−3] many theoretical studies have been performed to explain the extraordinary survival times for these quantum features.[4−17] In the experiments at 77 K, it was found that a beating pattern in 2D electronic spectroscopy survives for more than 1 ps, though in such a complex environment one would have expected much shorter decoherence times. Even at 277 K, a remnant of the oscillations is visible.[3] Under physiological conditions, the FMO complex forms a homotrimer, while recent crystal structures show that each monomer consists of eight bacteriochlorophyll (BChl) a molecules.[18] The eighth BChl which was overlooked for quite some time is only weakly bound to the complex. At least in some of the spectroscopic experiments, no spectroscopic signature of this eighth BChl is found,[19] which indicates that it dissolved from the complex while preparing the experimental samples. Also in simulations of the FMO monomer, the eighth BChl dissolved from the complex, though it was stable in the trimer simulations.[11,12]

Most of the calculations concerning the excitonic dynamics are based on site energies and spectral densities extracted from experiment (see, e.g., refs 5, 6, 9, 14, 16, 20, and 21), especially on the parameters by Adolphs and Renger[22] determined in a combination of theoretical and experimental information; recently, these parameters were extended to include the eighth BChl.[23] Other estimates for the spectral density were given by Cho and co-workers[24] and by Ishizaki and Fleming.[5] For the present study, all parameters are deduced from atomistic simulations.[11,12,25] These simulations were based on a combination of room-temperature molecular dynamics simulations and excited state calculations on the semiempirical ZINDO-CIS level including surrounding classical charges. From these calculations, the spectral densities as well as time-averaged site energies and couplings were deduced; a similar approach was recently pursued by Shim et al.[26] using molecular dynamics simulations combined with time-dependent density functional theory. It needs to be mentioned that the two computational results for the environmental effects[12,25,26] differ quite drastically. While one study seems to overemphasize the effect of the environment,[12,25] the other one apparently tends to underestimate it[26] if compared to the experimentally detected fluorescence sideband.[22,27] In the present study, we solely rely on the parameters extracted in refs 12 and 25, since we want to clarify the effect of initial preparations in a rather strongly damped system and demonstrate the possibility of coherent signatures *despite* strong dissipation. The influence of the corresponding differences in the parametrization of the site energies[12,23] on the exciton dynamics was also investigated recently.[13]

Various studies of the seven-[5,7,8,10,14] or eight-BChl monomer[15] or even the trimer[13] already used detailed parametrizations derived from numerical studies or spectroscopic data. The majority of these investigations relies on approximative schemes, e.g., second-order time-nonlocal master equations,[28] generalized Bloch−Redfield equations,[8] extended Lindblad approaches,[4] non-Markovian quantum jumps,[7] or an iterative linearized density matrix propagation scheme,[10] to name just a few. However, when attempting to give an exact account of quantum aspects of the excitation energy transfer (EET), the range of available methods is rather sparse. A

Received: February 13, 2012
Published: February 23, 2012

   dx.doi.org/10.1021/jp301444q | J. Phys. Chem. B 2012, 116, 3900−3906

variation of the time-dependent density matrix renormalization group method has recently been adapted to describe the EET dynamics in the framework of a dimer model at zero temperature,[29] while 2D spectra have been calculated for FMO monomers in the framework of hierarchical equations of motion,[17] and the quasiadiabatic propagator path integral scheme has been used to investigate population dynamics and entanglement in the FMO at different temperatures.[14] However, for modeling the protein and solvent environment, these works all rely on rather simple-structured spectral densities like a Drude–Lorentz form[17,29] or a superohmic form augmented by a single vibrational mode.[14]

In contrast, in this contribution, we take advantage of the rich information content available through recent atomistic modeling by employing numerically exact path integral Monte Carlo (PIMC) simulations to calculate the time-dependent population transfer using detailed spectral densities for each individual chromophore. With the full quantum dynamics of the EET at hand, we discuss the possibility of quantum coherent motion in the presence of a strong dissipative environment.

DESCRIPTION OF THE SYSTEM

The present work investigates the EET in a FMO monomer. As mentioned above, no spectroscopic signatures of BChl 8 were found in recent experiments,[19] and BChl 8 dissolved from the complex in the monomer simulations.[11,12] Accordingly, the monomer is described by a tight-binding model with $N = 7$ localized sites, corresponding to the seven BChls as depicted in Figure 1.

The protein scaffold and the surrounding solvent are treated as a dissipative environment in the spirit of the Caldeira–Leggett model,[30,31] i.e., as a set of harmonic modes bilinearly coupled to the electronic dipole moment. Though cross-correlations between these thermal reservoirs of each BChl have been extensively discussed in the literature,[6,20,21,32−35] in recent independent atomistic simulations, no spatial correlations between the fluctuations at different sites were observed.[11,26] Therefore, the environmental modes coupling to each individual BChl are regarded as being completely independent, leading to the Hamiltonian[22,36]

$$H = H_{\mathrm{BChl}} + H_{\mathrm{I}} + \sum_{n=1}^{N} H_{\mathrm{R}}^{(n)} \tag{1}$$

where

$$H_{\mathrm{BChl}} = \sum_{n=1}^{N} \varepsilon_n |n\rangle\langle n| + \sum_{n\neq m=1}^{N} \Delta_{nm} |n\rangle\langle m| \tag{2}$$

describes the bare BChl system with site energies ε_n and intersite couplings Δ_{nm} as the carrier of energy excitations,

$$H_{\mathrm{I}} = \sum_{n=1}^{N} |n\rangle\langle n| \left(\sum_{\alpha} c_{n\alpha} X_{n\alpha} + \Lambda_n^{(\mathrm{cl})} \right) \tag{3}$$

the coupling between the excitonic system and the protein–solvent environment with coupling constants $c_{n\alpha}$, and finally the thermal reservoir for BChl n,

$$H_{\mathrm{R}}^{(n)} = \sum_{\alpha} \left(\frac{{P_{n\alpha}}^2}{2m_{n\alpha}} + \frac{1}{2} m_{n\alpha} {\omega_{n\alpha}}^2 {X_{n\alpha}}^2 \right) \tag{4}$$

In these expressions, $X_{n\alpha}$, $P_{n\alpha}$, $m_{n\alpha}$, and $\omega_{n\alpha}$ are the position, momentum, mass, and frequency of the bath oscillators, respectively. Furthermore,

$$\Lambda_n^{(\mathrm{cl})} = \sum_{\alpha} \frac{{c_{n\alpha}}^2}{2m_{n\alpha}{\omega_{n\alpha}}^2} = \frac{\hbar}{\pi} \int_0^{\infty} \mathrm{d}\omega \frac{J_n(\omega)}{\omega} \tag{5}$$

denotes the classical reorganization energy of the reservoir connected to BChl n in terms of its spectral density

$$J_n(\omega) = \frac{\pi}{\hbar} \sum_{\alpha} \frac{{c_{n\alpha}}^2}{2m_{n\alpha}\omega_{n\alpha}} \delta(\omega - \omega_{n\alpha}) \tag{6}$$

As the values for the BChl energies ε_n are obtained from combined quantum-classical simulations for the full FMO–solvent complex, we included the reorganization energy $\Lambda_n^{(\mathrm{cl})}$ as a "counterterm"[30,31] in H_{I} (3) to prevent a further renormalization of the ε_n by the environment. The spectral densities comprise all information of the reservoirs necessary to access the full excitonic dynamics and can be obtained from the (classical) autocorrelation function of the energy gap fluctuation as described previously.[25,37] We note in passing that the definition of the spectral density here differs from the one used in ref 25 by a factor of $\pi/\hbar$.

With the electronic site energies ε_n, couplings Δ_{nm}, and the spectral densities $J_n(\omega)$ from ref 12 and Table S2 of ref 25 at hand, the quantum dynamics of the time-dependent BChl populations can be calculated according to

$$P_n(t) = \mathrm{tr}\{|n\rangle\langle n|\rho(t)\} = \langle n|\rho(t)|n\rangle = \rho_{nn}(t) \tag{7}$$

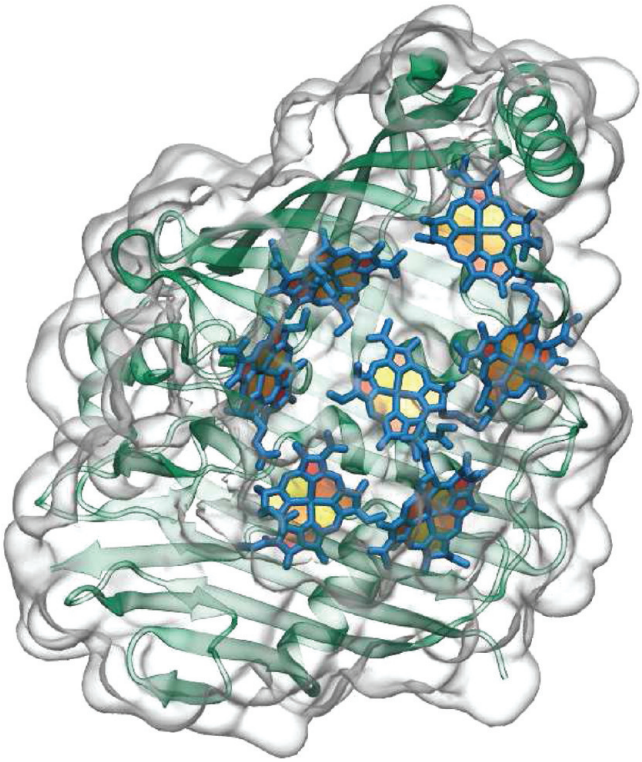

Figure 1. FMO monomer: Shown are the BChl molecules (in blue) without their pythyl tails embedded in the protein environment.

dx.doi.org/10.1021/jp301444q | J. Phys. Chem. B 2012, 116, 3900−3906

where the reduced density operator

$$\rho(t) = \mathrm{tr}_R\{W(t)\} \tag{8}$$

is obtained from the full system's density operator $W(t)$ by tracing over all reservoirs. In addition to the mentioned parameters, the evaluation of eq 7 also requires one to specify the state of the full system at some initial time point $t = 0$. Since the excitation processes in the corresponding experiments are usually performed with ultrashort laser pulses,[1−3] $W(0)$ can be assumed to factorize with respect to the BChls and the reservoirs

$$W(0) = \rho^{(0)} \bigotimes_{n=1}^{N} Z_R^{(n)-1} e^{-\beta H_R^{(n)}},$$
$$Z_R^{(n)} = \mathrm{tr}_R^{(n)}\{e^{-\beta H_R^{(n)}}\} \tag{9}$$

where $\mathrm{tr}_R^{(n)}$ denotes the trace over the nth reservoir in thermal equilibrium, while, e.g., for an excitation localized on BChl n_0, $\rho^{(0)} \equiv \rho(t = 0) = |n_0\rangle\langle n_0|$. While completely neglecting the initial system-bath correlations is somewhat unphysical and can even violate positivity (see ref 38 and references therein), for electronic excitation processes, it yields a reasonable initial description of the combined system.[28]

PATH INTEGRAL MONTE CARLO APPROACH

With all microscopic parameters and site-dependent spectral densities at hand, we can now extract the full quantum dynamics of the EET using PIMC simulations (for details, see ref 39 and references therein). In short, PIMC provides a numerically exact approach to access the time evolution of the reduced density matrix of dissipative quantum systems by stochastically sampling the path integral representation of the propagators in the framework of the Feynman−Vernon theory[40] or its extension to correlated initial preparations.[38] It can be applied for any system parameters and arbitrary spectral densities and is only limited by the computational effort necessary to obtain statistically converged results. Due to the notorious "dynamical sign problem",[41] which stems from interferences between different quantum paths, the corresponding numerical effort increases exponentially with the time scale over which the system's time evolution is investigated. For dissipative systems, however, efficient optimization schemes substantially soothe this computational bottleneck and significantly extend the accessible time scales.[42−44]

RESULTS AND DISCUSSION

Shown in Figure 2 are the different spectral densities for the individual BChls together with an average version, as reported in ref 25. It is clearly visible that the amplitudes of the spectral densities show drastic variations; e.g., those of BChl 4 and BChl 5 differ by more than a factor of 2. The population dynamics of the EET at room temperature (T = 300 K) for a single excitation initially localized at the "receiving" BChl 1 or 6, respectively, is shown in Figures 3 and 4. The decay of the initial excess population takes place on a picosecond time scale; however, the population dynamics due to an initial localization on BChl 6 are considerably faster both because of the differences in the coupling strengths between the various BChls (see also inset of Figure 4) as well as due to the weaker spectral density of BChl 6 compared to $J_1(\omega)$ (cf. Figure 2). This especially holds for the transfer speed toward BChl 3: For an excitation initially localized on BChl 6, the population of

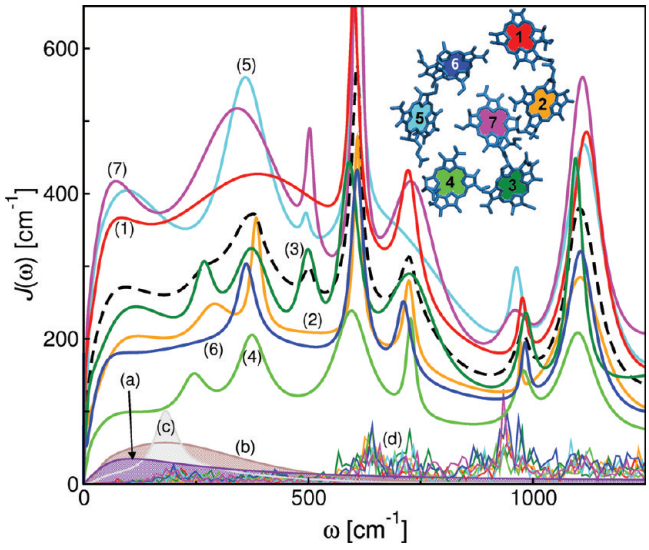

Figure 2. Spectral densities $J_n(\omega)$ for the individual BChls 1−7 of a FMO monomer; colors are chosen according to the schematic FMO shown on top (also labeled "(1)" to "(7)"). The average spectral density $J_{av}(\omega)$ is denoted by the black dashed curve. The reorganization energies (5) belonging to $J_1(\omega)$ to $J_7(\omega)$ are 84.1, 44.3, 54.2, 25.6, 86.9, 40.6, and 94.8 meV, respectively (average: 61.5 meV). In comparison are shown the spectral densities from Ishizaki and Fleming[5] (filled pink, (a)), Adolphs and Renger[22] (filled brown, (b)), Nalbach et al.[14] (filled gray, (c)), as well as Shim et al.[26] (d).

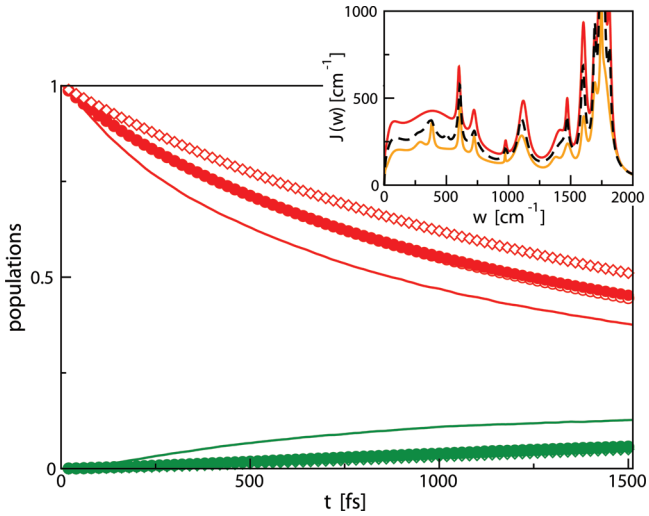

Figure 3. Population for the FMO monomer for sites 1 (red) and 3 (green). Filled circles denote PIMC results, thick lines corresponding data from ensemble-averaged wavepacket dynamics. Open circles and diamonds show PIMC results for averaged spectral densities $J_{av}(\omega)$ and a shifted bath preparation (10), respectively. The inset shows $J_1(\omega)$, $J_3(\omega)$, and $J_{av}(\omega)$ (red, green, and black, respectively).

BChl 3, $P_3(t)$, grows three times as fast as for an initial localization on BChl 1.

With respect to the individual BChls, the spectral densities obtained from atomistic modeling[25] are similar but do differ quantitatively. To illuminate to which extent differences in the site-resolved spectral densities influence the excitation dynamics, Figures 3 and 4 also include the population dynamics based on describing all seven reservoirs by the same averaged spectral density, $J_n(\omega) \rightarrow J_{av}(\omega) = (1/7)\sum_{n=1}^{7} J_n(\omega)$. For an initial localization on BChl 1, this loss of details has almost no

dx.doi.org/10.1021/jp301444q | J. Phys. Chem. B 2012, 116, 3900−3906

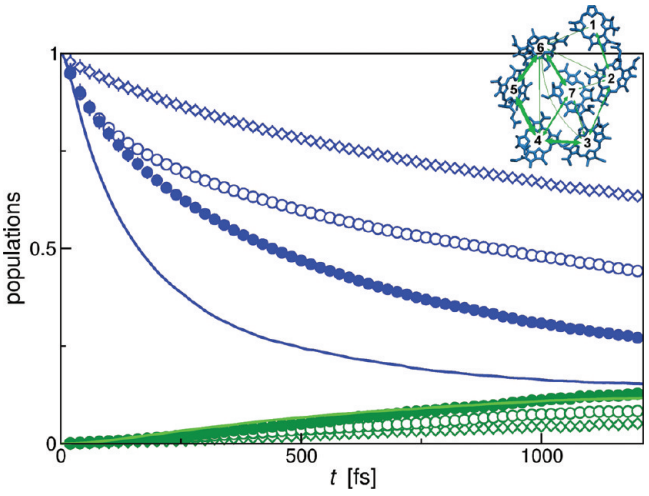

Figure 4. Same as Figure 3 but with the exciton initially localized on site 6 (blue). The inset shows couplings (green lines) between the BChls larger than 1 meV, with their thickness being proportional to $|\Delta_{nm}|$.

consequences at all on the transfer efficiency toward BChl 3, neither on the depopulation of BChl 1. This can be rationalized by noting that the transfer from BChl 1 to 3 can be effectively described by a three-state model BChl1 ↔ BChl2 ↔ BChl3[5,15] (see also Figure 5), and that for the (incoherent) initial step from BChl 1 to 2, which requires the reorganization of the reservoirs of both BChls, $\Lambda_1^{(cl)} + \Lambda_2^{(cl)}$ is almost invariant under replacing the individual spectral densities by $J_{av}(\omega)$ (cf. inset of Figure 3). By a similar argument, one would expect the transfer from BChl 2 to 3 to slow down, yet this is counterbalanced by a substantial mitigation of the population transfer from BChl 3 to 4, as the replacement of $J_4(\omega)$ by $J_{av}(\omega)$ significantly increases the activation barrier for this process. For the dynamics following an initial localization on BChl 6, however, the details of the spectral densities are quite relevant, as the latter effect leads to an impairment of the overall transfer to BChl 3 by about 40% (cf. Figure 4) and a simultaneous slowdown of the depopulation of BChl 6. Accordingly, in this case, dropping the individual spectral densities in favor of uniform $J_n(\omega) = J_{av}(\omega)$ results in a considerable diminuition of the transfer efficiency.

In addition, Figures 3 and 4 compare the numerically exact PIMC results with those obtained from ensemble-averaged wavepacket dynamics also denoted as Ehrenfest dynamics[45] (without back reaction of the relevant system on the thermal bath), which were performed analogously to ref 12 but on the monomer data. Recently, such approximative Ehrenfest dynamics have been discussed in comparison with results from a non-Markovian master equation in second-order approximation for smaller test systems.[46] For an initial excitation in BChl 1, the ensemble-averaged wave packet dynamics yields a comparable dynamics though displaying a decay which is somewhat too fast. The deviation becomes considerably larger for an excitation initially localized at BChl 6. These results once more demonstrate that Ehrenfest dynamics without back reaction is only valid for small to moderate system-bath coupling strengths.

The results shown so far all coincide in that they do not show any oscillatory excitonic behavior. In fact, neither for an initial localization of the excitation in BChl 1 or 6 nor for any other localized initial preparation do the excitonic populations exhibit anything but strictly incoherent dynamics even for short time

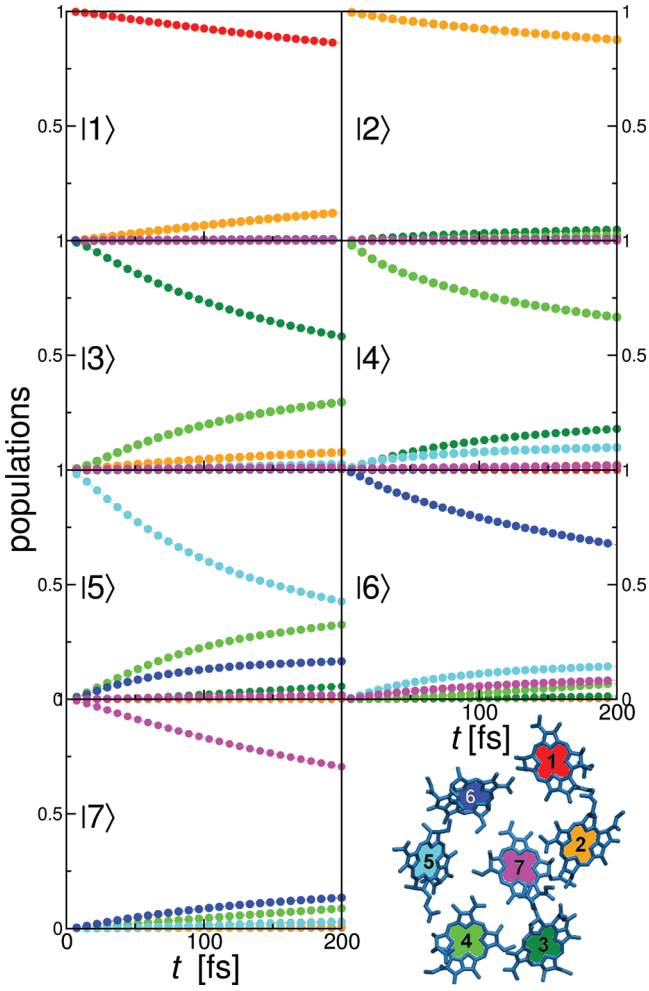

Figure 5. PIMC results for the short-time dynamics for an excitation initially localized on BChl n_0, with $|n_0\rangle$ as denoted in the panels; the color of the data points refer to the individual BChls as specified in the schematic FMO in the bottom right corner.

scales (cf. Figure 5). This seems to be in clear contradiction to recent experimental findings where at T = 277 K traces of coherent dynamics of about one oscillatory period could still be extracted,[3] as well as other theoretical works[5,10,14−16] which reported pronounced oscillatory behavior in the population dynamics after localization on BChl 1 or 6 even at room temperature. The latter can be accounted for by a different parametrization of the respective model Hamiltonians: The majority of previous theoretical studies employs spectral densities which, in the most relevant frequency range of up to about 500 cm^{-1}, are significantly lower (cf. Figure 2), thus leading to much weaker dissipation and correspondingly longer decoherence time scales. It has to be clarified that, in the spectral densities based on classical molecular dynamics simulations, the values above 500 cm^{-1} are severely over-populated due to the equipartition theorem of classical statistical mechanics; however, this is expected to have rather minor consequences with regard to the excitonic dynamics.[31] At the same time, there are only small contributions originating from vibrations belonging to the chromophores themselves in the above-mentioned low-frequency regime.[25] As the environment of the excitonic system not only consists of the protein scaffold of the FMO but also of surrounding solvent molecules, it seems noteworthy that, at all temperatures, the mentioned

dx.doi.org/10.1021/jp301444q | J. Phys. Chem. B 2012, 116, 3900−3906

experiments were conducted in 65% glycerol and 35% aqueous solution, of which the latter also contains 0.1% by mass lauryldimethylamine oxide (LDAO) which is known to form micelles around the proteins in the solution.[2,3] Both the formation of micelles as well as the partial replacement of water with the rather inert glycerol is expected to result in a significantly weaker coupling between the excitonic system and the fluctuating solvent, correspondingly diminishing the solvent's contribution to the spectral density. In determining the spectral density employed here, however, only water was used as the environment of the protein treated using a nonpolarizable force field,[12] and it therefore should be regarded as an "upper bound" for the strength of dissipation in the context of the recent experiments.

Apart from a different modeling of the protein solvent, the experimental and our computational results so far also differ in how the system is prepared prior to the measurement process. With respect to the environment, this should be of minor relevance: *In vivo*, the assumption of the protein−solvent complex initially being in thermal equilibrium (9) is well justified, since the waiting time prior to a "recharging" of the FMO complex with a new excitation is much larger than the time scale during which the transfer from the baseplate toward the RC is completed.[47,48] With regard to the 2D experiments, on the other side, one might argue in favor of a reconfiguration of environmental degrees of freedom due to the presence of an excitation in between the first and second laser pulse. However, even if the bath is initially fully equilibrated with respect to the initial localization of the excitation, i.e.,

$$\exp[-\beta H_{\mathrm{R}}^{(n_0)}] \rightarrow \exp[-\beta(H_{\mathrm{R}}^{(n_0)} - \langle n_0|H_{\mathrm{I}}|n_0\rangle)] \qquad (10)$$

in eq 9, again hardly any effects are visible for an initial localization on BChl 1, while for a preparation on BChl 6, the transfer efficiency toward BChl 3 once more decreases, yet still no coherent beating can be observed (cf. Figures 3 and 4).

Nevertheless, with regard to the excitonic setup, the situation is different: The laser pulses used in 2D spectroscopy prepare the BChl system in energy eigenstates[49] rather than creating localized excitations. Accordingly, Figure 6 presents the short-time population dynamics for the BChl system being initially in one of its energy eigenstates $|\psi_j\rangle$, $j = 1, \ldots, 7$. While the dynamics are still nonoscillatory, contrary to their counterpart with localized preparations (cf. Figure 5), they no longer exhibit a strictly monotonic convergence toward the respective equilibrium populations, and one might be tempted to interpret the transients as residues of coherent motion with frequencies between 50 and 100 fs. This is a direct consequence of the initial reduced density matrix being *nondiagonal* in the site representation.

To illuminate this purely preparational effect, we note that, in the *absence* of any dissipative influence, obviously coherent motion can only be observed if the density matrix, expressed in terms of the energy eigenbasis, exhibits some nonzero nondiagonal elements (aptly termed "coherences" in contrast to the "populations"[50]). However, in our case of a rather strong dissipative influence, the suitable basis to study dynamics is no longer given by the excitonic energy eigenstates, but rather by the pointer basis of the system-bath coupling,[51,52] i.e., the localized states $|n\rangle$. Again, with respect to the latter, a nondiagonal initial density matrix is more favorable than a diagonal one for observing coherent motion. As an excitation initially localized on a BChl n_0 refers to a diagonal $\rho_{nm}^{(0)} = \langle n|\rho^{(0)}|m\rangle = \delta_{nm}\delta_{mn_0}$, while a preparation in an energy eigenstate $|\psi_j\rangle$ leads to a nondiagonal $\rho_{nm}^{(0)} = \langle n|\psi_j\rangle\langle\psi_j|m\rangle$, the latter should be more suitable with respect to observing coherent dynamics.

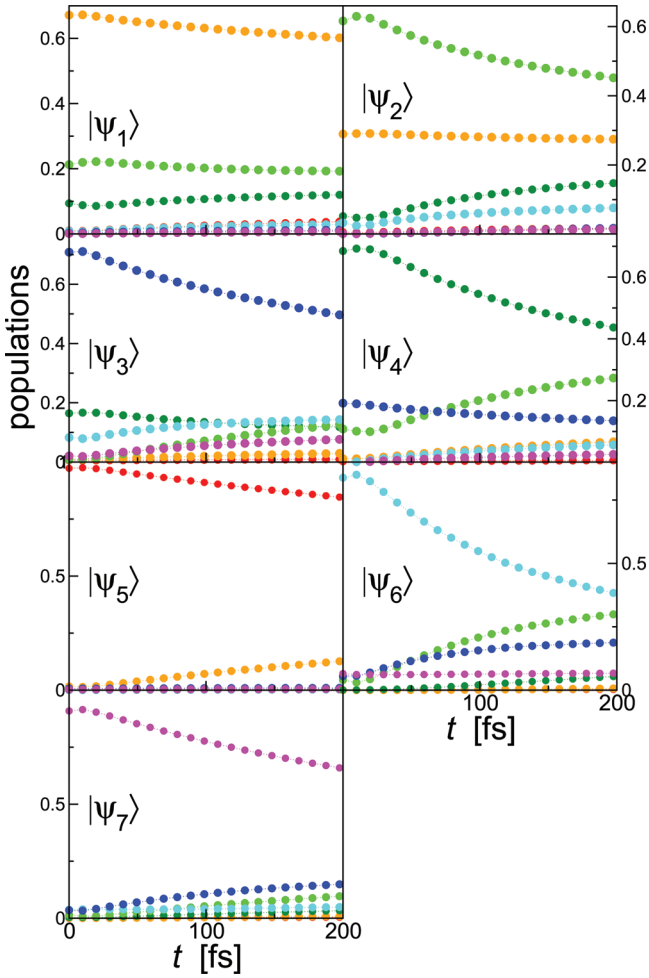

Figure 6. Same as Figure 5 but with the excitation initially prepared in an energy eigenstate $|\psi_j\rangle$ as denoted in the panels.

To underline this argument, we finally employ an initial preparation representing "maximal delocalization" of the excitation by using an uniform superposition of all localized states

$$\rho^{(0)} = |\phi\rangle\langle\phi|, \qquad |\phi\rangle = \frac{1}{\sqrt{7}}\sum_{n=1}^{7}|n\rangle \qquad (11)$$

such that the initial density matrix $\rho_{nm}^{(0)} = \langle n|\rho_0|m\rangle = 1/7 =$ const. has a pronounced nondiagonal character. Despite the rather strong dissipation, the corresponding dynamics, displayed in Figure 7, suddenly exhibit weak yet clearly visible traces of coherent motion, e.g., a full oscillation period in $P_5(t)$ and $P_7(t)$. In contrast, when dropping all the nondiagonal elements of $\rho_{nm}^{(0)}$ to recover a strictly diagonal density matrix $\tilde{\rho}_{nm}^{(0)} = \delta_{nm}\rho_{nm}^{(0)}$ describing a statistical mixture rather than a pure state, these oscillatory features completely vanish, and once more fully incoherent dynamics are obtained (cf. Figure 7). This demonstrates how, even in a strongly dissipative environment, coherent signals can be obtained by "optimizing" the initial preparation of the BChl system with respect to coherences in the initial reduced density operator $\rho^{(0)}$.

dx.doi.org/10.1021/jp301444q | J. Phys. Chem. B 2012, 116, 3900−3906

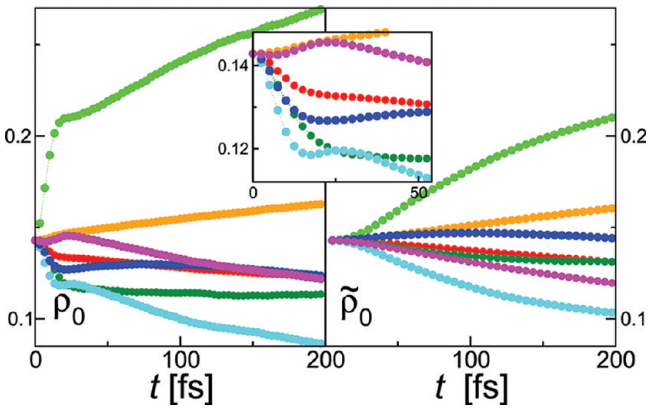

Figure 7. Same as Figure 5 but with the exciton being initially delocalized according to $\rho^{(0)}$ (eq 11, left panel) and $\tilde{\rho}^{(0)}$ (right panel). The inset enlarges the short-time dynamics for $\rho^{(0)}$.

SUMMARY

In the present work, parameters for the FMO complex from an atomistic simulation were combined with numerically exact PIMC calculations to study the quantum dynamics of EET at room temperature, with emphasis on the influence of preparational effects. While changes in the thermalization of the environmental modes show little effect on the transfer, switching from an initially localized excitation to the case of a delocalized one can induce traces of quantum beats up to a full oscillation period in otherwise incoherent dynamics. This clearly indicates the importance of initial coherences in the reduced density matrix of the BChl subsystem when discussing the relevance of quantum effects for EET in biological systems. However, these traces are rather weak in comparison to experimental findings; in addition, all localized preparations yield strictly incoherent dynamics, and PIMC simulations performed at 77 K, which will be the subject of a forthcoming publication, reveal a very similar picture. Although the population dynamics and the observed spectroscopic signals should not be expected to exhibit the exact same coherent−incoherent crossover, the present findings seem to strongly indicate that the spectral densities determined by the mentioned atomistic simulations do overestimate the dissipative influence of the environment. In ref 25, it is shown that, in the important low frequency regime, the spectral densities depend almost exclusively on the surrounding solvent rather than the internal modes of the protein scaffold. In the experiments, the protein is surrounded by a glycerol−water mixture including the micelle-forming LDAO, which is certainly different from the pure water solvent used in ref 25. However, also the treatment of the environment in the combined quantum-classical calculations might need further investigations. Clearly, the variations in the spectral densities for the individual chromophores do matter in the corresponding population dynamics.

Despite these differences with respect to modeling the environment, the present study clearly shows that preparational effects of the excitonic subsystem should be carefully taken into regard when comparing theoretical and experimental results, or the *in vivo* with the *in vitro* situation, since an initial delocalization of the excitation can significantly enhance the observability of quantum coherent motion in the FMO complex and even provoke a transition from incoherent to coherent dynamics in the presence of strong dissipation.

AUTHOR INFORMATION

Corresponding Author

*E-mail: lothar.muehlbacher@physik.uni-freiburg.de (L.M.); u.kleinekathoefer@jacobs-university.de (U.K.).

Notes

The authors declare no competing financial interest.

ACKNOWLEDGMENTS

We thank Mortaza Aghtar for help with the wave function-based results and Joachim Ankerhold, Heinz-Peter Breuer and Carsten Olbrich for insightful discussions. L.M. acknowledges financial support by grant MU 2926/1-1 of the Deutsche Forschungsgemeinschaft (DFG) and computational resources from the Black Forest Grid at the University of Freiburg.

REFERENCES

(1) Brixner, T.; Stenger, J.; Vaswani, H. M.; Cho, M.; Blankenship, R. E.; Fleming, G. R. *Nature* **2005**, *434*, 625−628.
(2) Engel, G. S.; Calhoun, T. R.; Read, E. L.; Ahn, T. K.; Mancal, T.; Cheng, Y. C.; Blankenship, R. E.; Fleming, G. R. *Nature* **2007**, *446*, 782−786.
(3) Panitchayangkoon, G.; Hayes, D.; Fransted, K. A.; Caram, J. R.; Harel, E.; Wen, J.; Blankenship, R. E.; Engel, G. S. *Proc. Natl. Acad. Sci. U.S.A.* **2010**, *107*, 12766−12770.
(4) Palmieri, B.; Abramavicius, D.; Mukamel, S. *J. Chem. Phys.* **2009**, *130*, 204512.
(5) Ishizaki, A.; Fleming, G. R. *Proc. Natl. Acad. Sci. U.S.A.* **2009**, *106*, 17255−17260.
(6) Caruso, F.; Chin, A. W.; Datta, A.; Huelga, S. F.; Plenio, M. B. *J. Chem. Phys.* **2009**, *131*, 105106.
(7) Rebentrost, P.; Chakraborty, R.; Aspuru-Guzik, A. *J. Chem. Phys.* **2009**, *131*, 184102.
(8) Wu, J.; Liu, F.; Shen, Y.; Cao, J.; Silbey, R. J. *New J. Phys.* **2010**, *12*, 105012.
(9) Abramavicius, D.; Mukamel, S. *J. Chem. Phys.* **2010**, *133*, 064510.
(10) Huo, P.; Coker, D. F. *J. Chem. Phys.* **2010**, *133*, 184108.
(11) Olbrich, C.; Strümpfer, J.; Schulten, K.; Kleinekathöfer, U. *J. Phys. Chem. B* **2011**, *115*, 758−764.
(12) Olbrich, C.; Jansen, T. L. C.; Liebers, J.; Aghtar, M.; Strümpfer, J.; Schulten, K.; Knoester, J.; Kleinekathöfer, U. *J. Phys. Chem. B* **2011**, *115*, 8609−8621.
(13) Ritschel, G.; Roden, J.; Strunz, W. T.; Aspuru-Guzik, A.; Eisfeld, A. *J. Phys. Chem. Lett.* **2011**, *2*, 2912−2917.
(14) Nalbach, P.; Braun, D.; Thorwart, M. *Phys. Rev. E* **2011**, *84*, 041926.
(15) Moix, J.; Wu, J.; Huo, P.; Coker, D. F.; Cao, J. *J. Phys. Chem. Lett.* **2011**, *2*, 3045−3052.
(16) Panitchayangkoona, G.; Voronineb, D. V.; Abramaviciusc, D.; Carama, J. R.; Lewisa, N. H. C.; Mukamel, S.; Engel, G. S. *Proc. Natl. Acad. Sci. U.S.A.* **2011**, *108*, 20908−20912.
(17) Hein, B.; Kreisbeck, C.; Kramer, T.; Rodríguez, M. *New J. Phys.* **2012**, *14*, 023018.
(18) Tronrud, D. E.; Wen, J.; Gay, L.; Blankenship, R. E. *Photosynth. Res.* **2009**, *100*, 79−87.
(19) Hayes, D.; Engel, G. S. *Biophys. J.* **2011**, *100*, 2043−2052.
(20) Nalbach, P.; Eckel, J.; Thorwart, M. *New J. Phys.* **2010**, *12*, 065043.
(21) Fleming, G. R.; Huelga, S.; Plenio, M. *New J. Phys.* **2010**, *12*, 065002.
(22) Adolphs, J.; Renger, T. *Biophys. J.* **2006**, *91*, 2778−2787.
(23) Schmidt am Busch, M.; Müh, F.; Madjet, M. E.; Renger, T. *J. Phys. Chem. Lett.* **2011**, *2*, 93−98.
(24) Cho, M.; Vaswani, H. M.; Brixner, T.; Stenger, J.; Fleming, G. R. *J. Phys. Chem. B* **2005**, *109*, 10542−56.
(25) Olbrich, C.; Strümpfer, J.; Schulten, K.; Kleinekathöfer, U. *J. Phys. Chem. Lett.* **2011**, *2*, 1771−1776.

(26) Shim, S.; Rebentrost, P.; Valleau, S.; Aspuru-Guzik, A. *Biophys. J.* **2012**, *102*, 649−660.
(27) Wendling, M.; Pullerits, T.; Przyjalgowski, M. A.; Vulto, S. I. E.; Aartsma, T. J.; Grondelle, R. v.; Amerongen, H. v. *J. Phys. Chem. B* **2000**, *104*, 5825−5831.
(28) Ishizaki, A.; Fleming, G. R. *J. Chem. Phys.* **2009**, *130*, 234111.
(29) Prior, J.; Chin, A. W.; Huelga, S. F.; Plenio, M. B. *Phys. Rev. Lett.* **2010**, *105*, 050404.
(30) Caldeira, A. O.; Leggett, A. J. *Ann. Phys.* **1983**, *149*, 374−456.
(31) Weiss, U. *Quantum Dissipative Systems*, 4th ed.; World Scientific: Singapore, 2012.
(32) Rebentrost, P.; Mohseni, M.; Aspuru-Guzik, A. *J. Phys. Chem. B* **2009**, *113*, 9942−9947.
(33) Nazir, A. *Phys. Rev. Lett.* **2009**, *103*, 146404.
(34) Fassioli, F.; Nazir, A.; Olaya-Castro, A. *J. Phys. Chem. Lett.* **2010**, *1*, 2139−2143.
(35) Strümpfer, J.; Schulten, K. *J. Chem. Phys.* **2011**, *134*, 095102.
(36) Yang, M.; Fleming, G. R. *Chem. Phys.* **2002**, *275*, 355−372.
(37) Damjanovíc, A.; Kosztin, I.; Kleinekathöfer, U.; Schulten, K. *Phys. Rev. E* **2002**, *65*, 031919.
(38) Grabert, H.; Schramm, P.; Ingold, G.-L. *Phys. Rep.* **1988**, *168*, 115−207.
(39) Mühlbacher, L.; Ankerhold, J.; Escher, C. *J. Chem. Phys.* **2004**, *121*, 12696−12707.
(40) Feynman, R. P.; Vernon, F. L. *Ann. Phys. (N.Y.)* **1963**, *24*, 18.
(41) Suzuki, M., Ed. *Quantum Monte Carlo Methods in Condensed Matter Physics*; World Scientific: Singapore, New Jersey, London, Hong Kong, 1993.
(42) Mak, C. H.; Egger, R. *Adv. Chem. Phys.* **1996**, *93*, 39.
(43) Egger, R.; Mühlbacher, L.; Mak, C. H. *Phys. Rev. E* **2000**, *61*, 5961.
(44) Stockburger, J.; Grabert, H. *Phys. Rev. Lett.* **2002**, *88*, 170407.
(45) Parandekar, P. V.; Tully, J. C. *J. Chem. Theory Comput.* **2006**, *2*, 229−235.
(46) Ishizaki, A.; Fleming, G. R. *J. Phys. Chem. B* **2011**, *115*, 6227−6233.
(47) Wen, J.; Zhang, H.; Gross, M. L.; Blankenship, R. E. *Proc. Natl. Acad. Sci. U.S.A.* **2009**, *106*, 6134−6139.
(48) Milder, M. T.; Brüggemann, B.; van Grondelle, R.; Herek, J. L. *Photosynth. Res.* **2010**, *104*, 257−264.
(49) Abramavicius, D.; Palmieri, B.; Voronine, D. V.; Sanda, F.; Mukamel, S. *Chem. Rev.* **2009**, *109*, 2350−2358.
(50) Sakurai, J. J. *Modern Quantum Mechanics*; Addison Wesley: Reading, MA, 1993.
(51) Zurek, W. H. *Phys. Rev. D* **1981**, *24*, 1516.
(52) Breuer, H. P.; Petruccione, F. *The Theory of Open Quantum Systems*; Oxford University Press: Oxford, U.K., 2002.